10-1998

WIYN Open Cluster Study. I. Deep Photometry of NGC188

Ted von Hippel
Embry-Riddle Aeronautical University, vonhippt@erau.edu

Ata Sarajedini
San Francisco State University

THE ASTRONOMICAL JOURNAL, 116:1789–1800, 1998 October

WIYN OPEN CLUSTER STUDY. I. DEEP PHOTOMETRY OF NGC 188

TED VON HIPPEL[1]
Department of Astronomy, University of Wisconsin, 475 North Charter Street, Madison, WI 53706; ted@noao.edu
AND
ATA SARAJEDINI
Department of Physics and Astronomy, San Francisco State University, 1600 Holloway Avenue, San Francisco, CA 94132; ata@stars.sfsu.edu
Received 1998 April 27; revised 1998 June 11

ABSTRACT

We have employed precise and carefully calibrated V- and I-band photometry of NGC 188 at WIYN Observatory to explore the cluster luminosity function (LF) and study the cluster white dwarfs. Our photometry is offset by $V = 0.052$ (fainter) from that of Sandage and Eggen & Sandage. All published photometry for the past three decades has been based on these two calibrations, which are in error by 0.05 ± 0.01. We employ the Pinsonneault et al. fiducial open cluster main sequence to derive a distance modulus of 11.43 ± 0.08 and $E(B-V) = 0.09$, with the largest single source of error caused by uncertainty in the cluster metallicity. We report observations that are $\geq 50\%$ complete along the main sequence to $V = 24.6$. We find that the NGC 188 central-field LF peaks at $M_I \approx 3$ to 4. This is unlike the solar neighborhood LF and unlike the LFs of dynamically unevolved portions of open and globular clusters, all of which typically rise continuously until $M_I \approx 9.5$. Although we find that $\geq 50\%$ of the unresolved objects in this cluster are multiple systems with mass ratios ≥ 0.3, their presence cannot account for the shape of the NGC 188 LF. For theoretical reasons having to do with the long-term survivability of NGC 188, we believe the cluster is highly dynamically evolved and that the low-luminosity stars missing from the central cluster LF are either in the cluster outskirts or have left the cluster altogether. We identify nine candidate white dwarfs (WDs) in NGC 188, of which we expect at least three, and perhaps six, are bona fide cluster WDs. The luminosities of the faintest likely WD indicate an age of 1.14 ± 0.09 Gyr, where the error in age includes the cluster distance uncertainty and we assume the WD has a hydrogen atmosphere. This age is a lower limit to the cluster age, and observations probing to $V = 27$ or 28 will be necessary to find the faintest cluster WDs and independently determine the cluster age. While our lower age limit is not surprising for this ≈ 6 Gyr–old cluster, our result demonstrates the value of the WD age technique with its very low internal errors.

Key words: Galaxy: stellar content — open clusters and associations: individual (NGC 188) — stars: luminosity function, mass function — white dwarfs

1. INTRODUCTION

NGC 188 has been the subject of frequent and intensive investigation primarily because of its great age. Many early studies (e.g., Sandage 1962; Eggen & Sandage 1969; Spinrad & Taylor 1969; Spinrad et al. 1970) were motivated largely by the belief that NGC 188 was approximately 10 Gyr old and therefore perhaps the oldest observable open cluster. Subsequent work has shown that the early age estimates were too large, with more modern values being typically 6 or 7 Gyr (e.g., Twarog & Anthony-Twarog 1989; Caputo et al. 1990; Demarque, Green, & Guenther 1992; Carraro et al. 1994; Dinescu et al. 1995). More modern work has also shown that other clusters, such as NGC 6791 and Berkeley 17 (see Phelps, Janes, & Montgomery 1994), are older than NGC 188. While NGC 188 has lost its pivotal role in constraining the age of the Galactic disk, it has still remained critically important for age studies since it is both nearer and less obscured than older clusters. Its metallicity is also typical of the solar neighborhood, with representative modern quotes of $[\mathrm{Fe/H}] = 0.02 \pm 0.11$ (Caputo et al. 1990), -0.12 ± 0.16 (Hobbs, Thorburn, & Rodriguez-Bell 1990), and -0.02 (Twarog, Ashman, & Anthony-Twarog 1997). Interest in NGC 188 has not been limited to its age and role in Galactic disk evolution, of course. A number of studies have looked at the cluster's wide giant branch (e.g., Twarog 1978; Norris & Smith 1985), blue stragglers (e.g., Leonard & Linnell 1992; Dinescu et al. 1996), and numerous W Ursae Majoris type and other contact binaries (e.g., van 't Veer 1984; Baliunas & Guinan 1985; Moss 1985; Kaluzny & Shara 1987; Kaluzny 1990). The great age of NGC 188 also means that cluster Lithium observations (e.g., Hobbs & Pilachowski 1988) can constrain stellar evolution and possibly cosmology. Extensive proper-motion observations (Upgren, Mesrobian, & Kerridge 1972; Dinescu et al. 1996) and radial velocity work (e.g., Scott, Friel, & Janes 1995; Mathieu & Dolan 1998) have also sought to help with cluster membership issues and the nature of the cluster's orbit in the Galaxy (e.g., Keenan, Innanen, & House 1973; Carraro & Chiosi 1994).

All of the above-quoted studies have necessarily been based on cluster members brighter than $V \approx 20$ and often brighter than $V \approx 15$. Our purposes in this paper were to add to our knowledge of NGC 188 based on the modern techniques of deep CCD photometry coupled with a large telescope. Specifically, we wanted to address the cluster luminosity function, which is the result of both the initial mass function (IMF) and the cluster dynamical evolution. Our goal was to observe to ~ 10 mag fainter than the

[1] National Optical Astronomy Observatories, 950 North Cherry Avenue, Tucson, AZ 85719.

TABLE 1

LOG OF OBSERVATIONS

Date (1)	Conditions (2)	V (3)	I (4)	Seeing (5)	Notes (6)
1995 Jul 10	NP	...	1.0	1.0–1.2	
1995 Jul 24–27	P	4.25	2.5	1.0–1.5	Standards but nonlinear
1996 Feb 4	P	...	2.0	0.7	No standards
1996 Aug 12–15.....	NP	2.5	3.75	1.2–2.0	Discarded
1996 Sep 19	P	1.5	1.0	0.9–1.6	Standards and postrepair

cluster turnoff, or to an equivalent mass of $\sim 0.2\,M_{\odot}$. These observations could then be compared with other deep photometry of open and globular clusters, obtained primarily with the *Hubble Space Telescope* (*HST*). We were able to achieve this goal in a central cluster field and discuss the ramifications for the dynamical evolution of NGC 188 below. We also sought to find the faintest possible cluster white dwarfs. Recent *HST* observations (von Hippel, Gilmore, & Jones 1995; Richer et al. 1997) have demonstrated that cluster white dwarfs are a powerful and independent means of determining the ages of star clusters. In addition, while completing this paper we came across a comparative study of open cluster distances based on *Hipparcos* (ESA 1997) parallax measurements and the main-sequence fitting technique (Pinsonneault et al. 1998), which allows us to independently rederive the distance to NGC 188. An independent distance to NGC 188 is important since there has been considerable difficulty and uncertainty in untangling the cluster's distance, reddening, and metallicity (see Twarog & Anthony-Twarog 1989). Finally, we do not fit isochrones, as the turnoff and giant branch are not well delineated in our data. Isochrone fitting will be the subject of a future paper, which will combine deep WIYN[2] data with wide-field photometry from the Kitt Peak 0.9 m telescope.

Our paper is also the first in what we hope will be a long and useful series of coordinated papers on open clusters relying heavily on WIYN data. With its 1° diameter field of view feeding a 100-fiber multiobject spectrograph, its high-quality imaging, and sizable aperture, WIYN is an ideal tool for open cluster work. To this end, a group of approximately a dozen researchers from the WIYN institutions and their collaborators have formed what we call the WIYN Open Cluster Study (WOCS). Our collaboration will study approximately 10 open clusters spanning the widest possible range of age and metallicity in great detail over the next decade, measuring Fe, C, O, Li, and hopefully N abundances, precise radial velocities, proper motions, and broadband colors. While the observations are to take place primarily at WIYN, we will also supplement and support our WIYN observations with other telescopes. We will present our results and data on-line (see http://www.astro.wisc.edu) as they are published.

2. DATA REDUCTION

We observed NGC 188 at the WIYN 3.5 m telescope on Kitt Peak through the Harris V-band and Mould interference I-band filters (Massey et al. 1987) over a 14 month period during runs ranging from a few hours to a few nights in duration. Table 1 lists the details of the observations including the four-night period 1996 August 12–15, when low transparency and poor seeing in the end made the observations too poor for our use. Column (1) of Table 1 lists the date(s) of the runs; column (2) lists the sky conditions, with "P" indicating a photometric night and "NP" indicating a nonphotometric night; columns (3) and (4) list the exposure times in hours in the V and I bands, respectively; column (5) lists the range of seeing for the run measured as the FWHM of a Gaussian fit; and column (6) provides notes to the runs. The table includes 11 nights, a few of which were partially allocated to this program. Of the cumulative 10 nights devoted to this project, owing to frequent bad weather and some problems with the CCD (discussed below), the final tally of useful observations was 5.75 hr of V-band exposure and 6.5 hr of I-band exposure. The image quality was also generally poorer than the median recorded at WIYN ($\sim 0\farcs8$ FWHM), ranging from $0\farcs7$ to $1\farcs6$ FWHM. Nonetheless, ~ 6 hr of exposure per filter with a 3.5 m telescope allows us to address a number of the goals as set out in § 1 and to present observations of this cluster to $V \approx 25$, 5 mag fainter than previous work.

The CCD detector currently in use at WIYN, "S2KB," is a 2048^2 STIS CCD with 21 μm ($=0\farcs197$) pixels and a field of view of $6\farcm72 \times 6\farcm72$. Observations were obtained near the center of NGC 188, at R.A. $= 0^{h}48^{m}26^{s}$, decl. $= +85°15'21''$ (J2000.0), corresponding to Galactic coordinates $(l,\ b) = (122\fdg9,\ +22\fdg4)$. Data reduction followed standard procedures although a few extra steps for the particular characteristics of the S2KB CCD were incorporated. In particular, this CCD has a time-dependent, two-dimensional bias structure that can range from ≈ 4 ADU to ≈ 20 ADU. The bias structure is typically stable within a few ADU on any given night, however. By fitting a polynomial of order ~ 4 to the overscan regions of all calibration and science frames and performing a residual bias subtraction, we were able to remove the bias offset and structure typically to within 2 ADU. The largest bias uncertainty was in the low-row, low column number region, a region we avoided using for the standard stars. For the deeper broadband (science) exposures, the high sky meant that this bias uncertainty was always much less than 1%. Flat-fielding was performed using dome flats with typical pixel-to-pixel Poisson uncertainties of less than 0.3% and illumination pattern uncertainties less than 1.0%.

All photometry over the past 30 years of NGC 188 with which we are familiar has been calibrated against Sandage (1962) and Eggen & Sandage (1969). Since photometric equipment and techniques have improved over the past 30 years, we decided to obtain our own photometric calibration at WIYN. Our early efforts were hampered by a (then unknown) severe nonlinearity in the S2KB CCD when

[2] The WIYN Observatory is a joint facility of the University of Wisconsin–Madison, Indiana University, Yale University, and the National Optical Astronomy Observatories.

this chip was exposed to background counts of less than $\approx$200 ADU (at an inverse gain setting of 2.8 e^- ADU^{-1}). The nonlinearity was background dependent and rose to 40% for point sources on a zero count background. We thus discarded our short calibration exposures taken during 1995 July 24–27 (Table 1) and reobserved NGC 188 on the photometric night of 1996 September 19 once the S2KB CCD had been repaired. On 1996 September 19, we also obtained 46 V-band observations of 25 Landolt (1983, 1992) standard stars and 40 I-band observations of 26 Landolt standard stars. These observations were reduced in the same manner as the data, although with the aperture corrections determined from the standard stars rather than from the bright program stars. We used the routine of Harris, Fitzgerald, & Reed (1981) to simultaneously fit a zero point, an air-mass term, and a first-order color term for each of V and I. The resulting photometric transformations were

$$V = v + 24.877 - 0.169X + 0.010(V-I)\,, \quad (1)$$

$$I = i + 24.271 - 0.065X + 0.031(V-I)\,, \quad (2)$$

where V and I are magnitudes in the standard system, v and i are magnitudes in the instrumental system, and X is the air mass.

After applying the above calibration to our data, we looked for a range of parameters that might correlate with the residuals in the photometry. Nothing we checked correlated with the photometric residuals except Universal Time (UT). Not only did we search for correlations using the standard-star data, but we also used many bright stars in the NGC 188 frames themselves (15 epochs) to look for the same correlations, since the entire night of 1996 September 19 was spent monitoring the same field in NGC 188 and standard stars. We found a highly significant, but small-valued, correlation between Universal Time and the residuals in both the NGC 188 stars and the standard stars. This correlation is shown in Figure 1. Since the NGC 188 observations cover a greater range in Universal Time, they better determined the slope of the UT versus residual V and I magnitude relations. The NGC 188 residual slope was imposed on the standard-star data. Figure 1 demonstrates that the NGC 188 and standard-star residual slopes were very similar, however. The best-fit correlations were

$$\mathrm{cor}\,(UT,\,V) = 0.1275 - 0.0125\,\mathrm{UT}(V), \quad (3)$$

$$\mathrm{cor}\,(\mathrm{UT},\,I) = 0.1020 - 0.010\,\mathrm{UT}(I)\,, \quad (4)$$

where cor(UT, V) and cor(UT, I) are the corrections to apply as a function of Universal Time in V and I, respectively, and UT(V) and UT(I) are the values of Universal Time during the observations in V and I, respectively. The additive constants in the above two equations zero-point the photometry to UT = 10.20. The NGC 188 data were offset to the same zero point as the standard stars.

We interpret the temporal dependence of the photometry as a slow and monotonic change in the atmospheric transparency. The final result had internal residuals of 0.004 mag for the V band and 0.009 mag for the I band. The color terms of 0.010 and 0.031 for V and I, respectively, were consistent with the color terms measured by our group during telescope commissioning and seen subsequently by other observers. Both the small residuals and the small color terms demonstrate that the WIYN Harris V and Mould interference I filters are on the Landolt Johnson-Kron-Cousins photometric system (see Landolt 1992). The atmospheric extinction terms are within the normal range of extinction terms seen at Kitt Peak.

In Figure 2, we compare our V-band data with that of Sandage (1962) and Eggen & Sandage (1969) as a function of apparent V-band magnitude and as a function of $V-I$ color. We find a mean offset of V(Eggen & Sandage) $-$ V(this work) $= -0.052$ mag with a standard deviation of 0.063 mag. For the 76 objects in common, the offset is highly significant. (When we compare our photometry to the 23 stars in common with Caputo et al. 1990 we find a mean offset of -0.059 and a standard deviation of 0.022. The similarity is expected since the Caputo et al. photometry was calibrated against the Eggen & Sandage photometry.) These data show no convincing trend between the difference of our photometry and that of Eggen & Sandage with either magnitude (Fig. 2*a*) or color (Fig. 2*b*). We attribute the systematic photometric difference between our work and that of Eggen & Sandage to possible differences in the photoelectric versus CCD passband and calibrations, as well as the difficulty of doing photometry at an

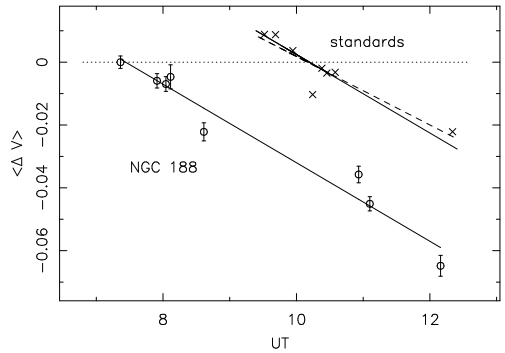

FIG. 1*a*

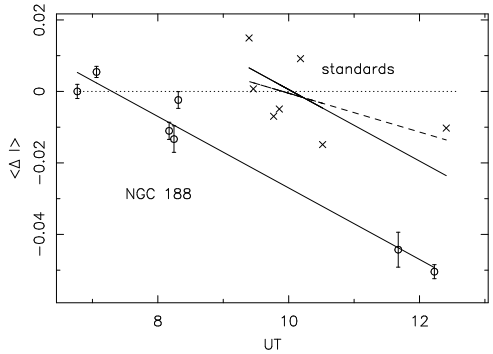

FIG. 1*b*

FIG. 1.—(*a*) Correlation between the Universal Time of observation and the mean V-band photometric residual after removing the first-order extinction and color terms. The error bars on the NGC 188 data points (*circles*) represent the standard deviation of at least 16 stars observed at that epoch. The mean value for the standards at each epoch are represented by crosses. The absolute difference in the standards and the relative difference in the NGC 188 data both yield essentially the same slope. The dashed line shows the slope fitted only to the standards, whereas the solid line shows the slope fitted to the NGC 188 data and imposed on the standard-star data. The zero point is set at UT = 10.20. (*b*) Same as (*a*), but for the I band.

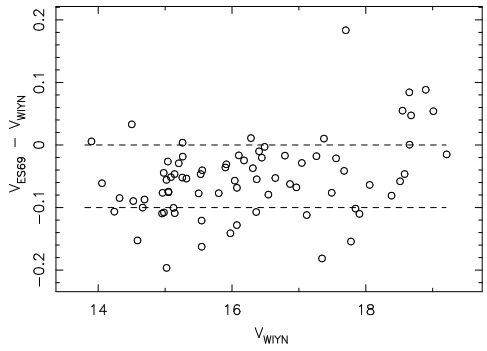

FIG. 2a

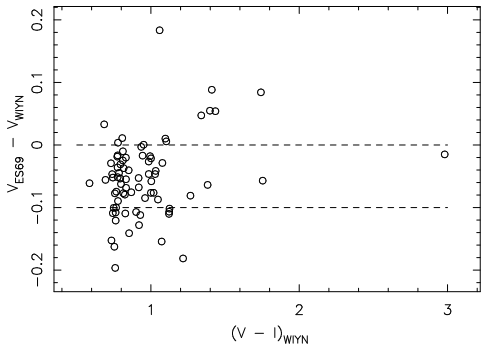

FIG. 2b

FIG. 2.—(*a*) Difference between the V-band photometry of Eggen & Sandage (1969) and our V-band photometry vs. apparent magnitude. Dashed lines at $\Delta V = 0.0$ and -0.1 are overplotted to aid the eye in comparing the photometry. (*b*) Same as (*a*), but plotted against $V-I$ color.

air mass of ≥ 1.7. As a further check, we compared V-band magnitudes for stars in common between our WIYN data and our (as yet) unpublished KPNO 0.9 m data, employing a calibration kindly provided by E. M. Green (1998, private communication). We found that these two independent calibrations agree to within 0.01 mag. We believe the modern filter prescription, our careful tying of the WIYN photometry to the Landolt system, and the modern ability to place multiple standard stars on the same CCD field allowed us to determine a more reliable photometric zero point than that of Sandage (1962) and Eggen & Sandage (1969).

For each of the observing runs (Table 1) we co-added the data within a given run using IRAF (Tody 1993) routines to register, scale, and offset the frames. Scaling and offsetting the frames before co-addition is necessary since the sky transparency and background change as a function of air mass even under photometric conditions. The resulting V- and I-band frames for each run were then fitted with a quadratically variable point-spread function (PSF) using the multiple-PSF fitting ALLFRAME reduction package (Stetson 1994; see below). We employ the PSF-fitting photometry rather than aperture photometry because of its optimum signal-to-noise weighting of the data, and not because of crowding. These images contain $\lesssim 10^4$ objects spread over 4×10^6 pixels, and so only a small percentage of the detected objects are blended with other objects.

For each combined image, we began by constructing a high signal-to-noise PSF using 50–100 bright uncrowded stars. We then established a spatial transformation between each combined image and a reference image using the DAOMASTER software, kindly provided by P. Stetson. We use this transformation to further combine all of the combined images to form one master frame to be used in defining a list of coordinates for all detected image profiles. The SExtractor (Bertin & Arnouts 1996; see below) source-finding routine was used to expedite this process. This master coordinate list was input into ALLFRAME along with the PSFs of each frame and the spatial transformation relation. The output of ALLFRAME consists of instrumental photometry for each detected profile on each frame as well as an image from which all of the profiles have been subtracted. We then combined all of these subtracted frames and used SExtractor to augment the original list of image profiles. This new master list of coordinates was again fed into ALLFRAME to yield the final list of instrumental magnitudes.

Because of the slight warpage of the S2KB CCD, the quadratically varying PSF did not fully account for the spatial variation of the PSF. To correct for this, we selected between 200 and 300 bright stars per epoch. After all of the other stars were subtracted from the frames, we performed large-aperture (radius = 25 pixels) photometry for all of these stars. The difference between the PSF magnitude and the aperture magnitude [cor (R)] was then plotted as a function of the distance from the lower left corner of the frame (R). The only frame that exhibited a large variation (± 0.05 mag) was the I frame taken on 1996 February 4. The others showed a very small ± 0.005 mag variation. In any case, we fitted polynomials of the form

$$\text{cor}\,(R) = a_0 + a_1 R + a_2 R^2 \qquad (5)$$

to the data using an iterative 2 σ rejection technique. These equations were applied to the instrumental magnitudes.

The photometry for each run was then merged and put on the Landolt standard system based on the bright, but unsaturated, stars that overlapped with the 1996 September 19 data set. The number of such stars ranged from 41 to 119 per run, and the residuals in the offset range from 0.015 to 0.03 mag.

Since a large number of the detected faint objects are not stars, but rather background galaxies, we also required a method to morphologically reject nonstellar objects. After careful comparison of visual and automated morphological rejection techniques we chose to use SExtractor (Bertin & Arnouts 1996). SExtractor has the advantage of determining sky locally and uses verified neural network techniques to perform the star/galaxy classification. Figure 3 shows the results of the SExtractor morphological classification versus I-band magnitude. The "stellarity index" ranges from 0 (galaxies) to 1 (stars). Although SExtractor's neural network classifier is not strictly a Bayesian classifier, the stellarity index values are approximately the probabilities that the object is a point source. The large number of definite stars in Figure 3 demonstrates that a cluster is present in this field, though there is significant contamination, especially at the faintest magnitudes. The large number of classifications near 0.5 at the faintest magnitudes demonstrates the commonsense notion that at limiting signal-to-noise ratio classification breaks down. SExtractor understands this and yields a sensible classification of ~ 0.5, i.e., unsure. Note also that saturated stars have an associated probability of being stellar of somewhat less than 0.9. This too is sensible

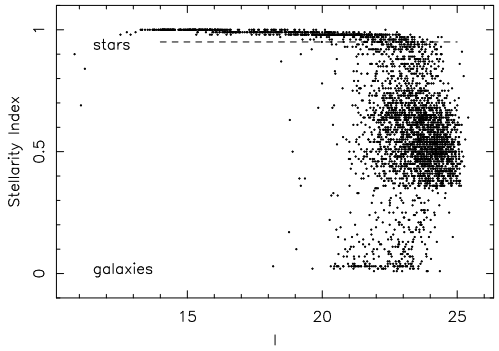

FIG. 3.—SExtractor (Bertin & Arnouts 1996) "stellarity index" classifications vs. I-band magnitude. The stellarity index ranges from 1.0 for definite stars to 0.0 for definite galaxies. The horizontal dashed line at 0.95 is our high-confidence star threshold. As expected, classification breaks down for the faintest objects.

behavior for SExtractor given that these stars have flat-topped, broader PSFs.

We select only those objects determined by SExtractor to have a high (≥ 0.95, marked by the dashed line in Fig. 3, i.e., $\gtrsim 95\%$) probability[3] of being stars and present their calibrated color-magnitude diagram (CMD) in Figure 4. Note that the requirement of a good morphological classification, which is somewhat different than simply signal-to-noise ratio, imposes the faint magnitude limit in Figure 4. Before moving on to a detailed discussion of the NGC 188 CMD we pause to point out that a strong binary sequence is evident in this cluster to the limit of the data and that the number of cluster stars drops markedly fainter than $V \approx 18$. The turnoff for this cluster is at $V \approx 15$ and the faintest stars, at $V = 25$, have masses $\lesssim 0.2\ M_{\odot}$ based on the empirical mass-luminosity relations of Henry & McCarthy (1993). Individual error bars are not plotted for clarity but typical photometric errors at each integer V-band magnitude starting at $V = 19$ are presented down the right-hand side of Figure 4. These errors are internal errors only.

We estimate the total systematic error of our photometry as due to the errors in the standard-star calibration and the errors in transforming the data taken under non-photometric conditions onto the single calibrated night. The external accuracy of the standard-star calibration should be excellent since the residuals about the final calibration were only 0.004 in V and 0.009 in I. Furthermore, dropping individual standard stars from the solution affected the transformation coefficients by always ≤ 0.003 mag. Note, however, that the reddest Landolt standard we used had $V-I = 2.08$, whereas our data continue to $V-I = 3$, and beyond. The color term for the lower main sequence is thus an extrapolation and is likely to be somewhat less accurate than the rest of the photometry. We estimate that our transformations blueward of $V-I = 2$ to the Landolt system are accurate to ≤ 0.01 mag. We further estimate that the procedures of calibrating subsequent photometry to the one calibrated night are accurate to 0.01 to 0.03 mag, depending on the epoch. Multiple observations for most stars will reduce the epoch-to-epoch variations, but we will use 0.03 mag as our error for this bootstrapping

[3] We performed careful visual examination of the images and found two galaxies and one location on a diffraction spike for which SExtractor reported stellarity ≥ 0.95. The misclassification is consistent with the probablistic nature of the classification and the stellarity ≥ 0.95 cutoff.

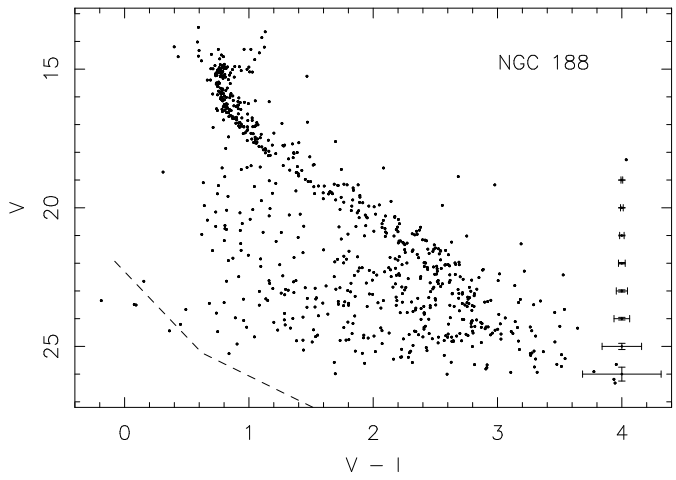

FIG. 4.—Calibrated color-magnitude diagram in V and I for NGC 188. Typical photometric errors at each integer V-band magnitude starting at $V = 19$ are presented down the right-hand side. Only objects with a likelihood $\gtrsim 95\%$ of being stars according to SExtractor are plotted. The loci of solar neighborhood white dwarfs in the trigonometric data of Monet et al. (1992), offset to the cluster distance and reddening, are overplotted as a dashed line.

calibration step. The overall external systematic in the photometry blueward of $V-I = 2$ should be ≤ 0.032.

3. DISCUSSION

3.1. *A New Distance Determination*

Past distance determinations (see Twarog & Anthony-Twarog 1989 for an extensive discussion) to NGC 188 have been based on the morphology of the turnoff, subgiant, and red giant regions fitted by stellar isochrones. These fits simultaneously determine the cluster distance, reddening, and age, while explicitly adopting a metallicity value and implicitly depending on a host of parameters in the stellar evolution models. Perhaps the most up-to-date and reliable value for the distance and reddening of NGC 188 is $m-M = 11.35$ and $E(B-V) = 0.09$ (Twarog et al. 1997).[4] These values update the results of Twarog & Anthony-Twarog (1989), who found $m-M = 11.50$ and $E(B-V) = 0.12$, which since 1989 have been the canonical cluster values. While Twarog & Anthony-Twarog (1989) and Twarog et al. (1997) have considered other constraints on the cluster distance and reddening besides fits to stellar evolutionary models, the precise distance and, especially, reddening still remain uncertain. It is our contention that the distance modulus is uncertain to ~ 0.10 mag and the reddening to ~ 0.03 mag. In addition, since our photometry is offset by $V = 0.052$ (fainter) from Sandage (1962) and Eggen & Sandage (1969), it is necessarily offset by the same value from the photometric distance determinations of all other studies since they were calibrated against Sandage (1962) and Eggen & Sandage (1969). For all of these reasons, and since we can provide a distance determination independent of previous techniques, we rederive the distance to NGC 188, below.

Our data precisely determine the main-sequence locus from the turnoff near $V = 15$ to the lower main sequence at least as faint as $V = 21$ (where $V-I \approx 2$, the interpolation

[4] We rely on the reddening relations of Cardelli, Clayton, & Mathis (1989) to convert $E(B-V)$ to $E(V-I)$; see below.

limitation of the Landolt standards). We would like to compare our photometry with the precise trigonometric parallaxes of solar-metallicity dwarf stars made by the *Hipparcos* (ESA 1997) mission. Since the *Hipparcos* satellite did not make photometric measurements in the Johnson-Kron-Cousins system, there is no directly determined fiducial main sequence for our filters. Fortunately, Pinsonneault et al. (1998) have just completed a detailed study of *Hipparcos* parallaxes to individual cluster members in five nearby open clusters (α Per, Coma Berenices, Hyades, Pleiades, and Praesepe) and they have derived just such a fiducial main sequence for solar-metallicity stars in both $B-V$ and $V-I$. Although Pinsonneault et al. find a systematic problem with the Pleiades parallaxes, they argue that the other four open clusters are consistent with the same fiducial sequence within very stringent limits. They conclude that with good data one can derive the distance to a near–solar-metallicity open cluster using the main-sequence fitting technique to an accuracy in the distance modulus of 0.05 mag. Since we have no independent means of determining the reddening to NGC 188, we derive the distance based on the two recent and most commonly quoted values, $E(B-V) = 0.09$ and 0.12. In Figures 5*a* and 5*b* we present our photometry in the region of the Pinsonneault et al. (1998) fiducial solar-metallicity main sequence (*solid lines*) for our best-fit distance of $m - M = 11.43$ for $E(B-V) = 0.09$ and $m - M = 11.67$ for $E(B-V) = 0.12$, respectively. The 1 σ error bars are plotted for the data, and fiducial sequences offset by ± 0.05 mag are presented as dashed lines.

We derived the cluster distance moduli by first selecting what appeared to be single-star cluster main-sequence members within the range $0.8 \leq V-I \leq 1.0$, i.e., unevolved main-sequence stars within the Pinsonneault et al. color calibration range [$(V-I)_0 \leq 0.9$]. These selected stars are indicated in Figure 5 by overplotted circles. We then slid the fiducial sequence vertically in 0.01 mag increments until the mean offset of the selected stars went to zero. Following this procedure we determined initial cluster distance moduli of $m - M = 11.41$ for $E(B-V) = 0.09$ and $m - M = 11.63$ for $E(B-V) = 0.12$. Since photometric binaries create a sequence of objects above and to the right of the main sequence, we then studied the distribution of our selected stars about the fiducial sequence for the initial cluster distance moduli. These distributions are plotted in Figures 6*a* and 6*b* for the $E(B-V) = 0.09$ and $E(B-V) = 0.12$ cases, respectively. One can clearly see in both figures that the stars do not constitute a normal distribution about the initial cluster distance moduli. Rather, a peak at negative offset values is present, as is a tail to positive offset values. This is precisely what we expect from the inclusion of unresolved binaries. We thus improve upon our initial distance estimate by including an offset of 0.02 and 0.04 mag to the peak in the single-star sequence for the two $E(B-V) = 0.09$ and 0.12 cases, respectively. We also performed these same tests with our unpublished KPNO 0.9 m photometry and found $m - M = 11.43$ for $E(B-V) = 0.09$ and $m - M = 11.58$ for $E(B-V) = 0.12$. The consistency between the WIYN and KPNO 0.9 m $E(B-V) = 0.09$ results is encouraging, as is the fact that they agree with the Twarog et al. (1997) results (recall the 0.05 mag offset in the photometric zero point). The 0.05 mag difference between the WIYN and KPNO 0.9 m $E(B-V) = 0.12$ results does not disfavor these results, since this difference is within the quoted errors of the technique and could anyway result from a departure from solar metallicity. We believe, however, that $m - M = 11.63$ is too high given the extensive past work on the cluster distance, while at the same time the lower reddening seems to be preferred by Twarog et al. (1997). We thus rely on $m - M = 11.43$ and $E(B-V) = 0.09$ for the remainder of this paper.

The quality of our photometry is good enough that we adopt the 0.05 mag precision for this distance technique quoted by Pinsonneault et al. (1998). One external error to consider is uncertainty in the ratio of $E(V-I)$ to $E(B-V)$. We rely on equations (3a) and (3b) of Cardelli et al. (1989) to derive a value of 1.34 for the central wavelength (8220 Å) of our I-band filter. This may be mildly inconsistent with Pinsonneault et al., who use $E(V-I) = 1.25E(B-V)$, though we cannot be sure as we do not know the central wavelength(s) for the I-band photometry they have collected. We estimate this source of uncertainty at a given $E(B-V)$ value to be only of order 0.01. Another source of external error is the external accuracy of our photometry. We argued above that this should be ≤ 0.032. Yet another

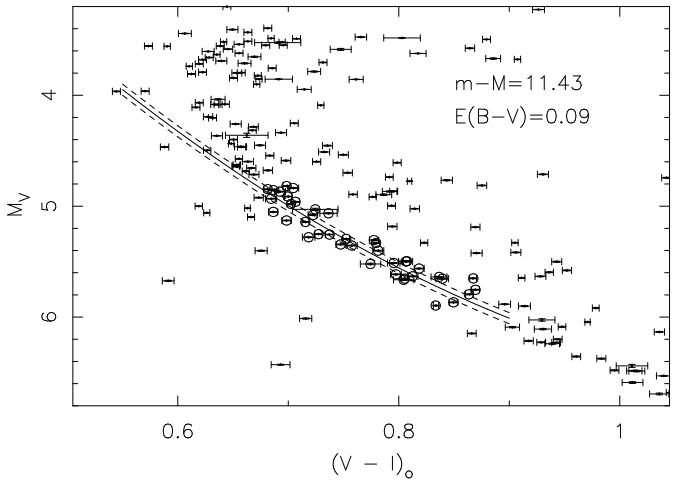

FIG. 5*a*

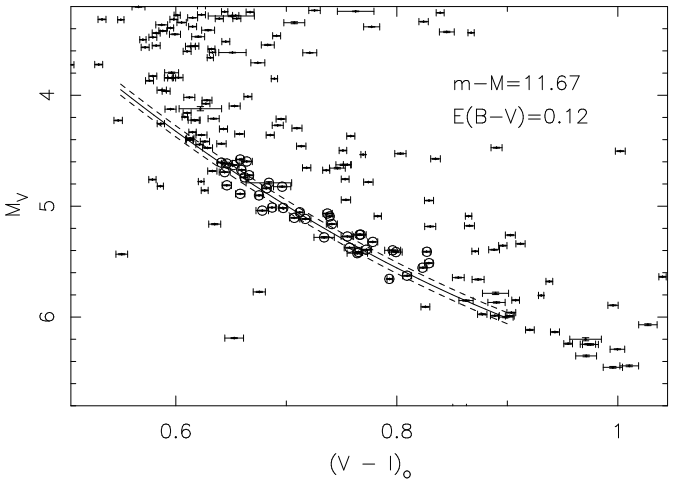

FIG. 5*b*

FIG. 5.—(*a*) Our photometry in the region of the Pinsonneault et al. (1998) fiducial solar-metallicity main sequence (*solid line*) for our best-fit distance of $m - M = 11.43$ for $E(B-V) = 0.09$. The 1 σ error bars are plotted for the data, and fiducial sequences offset by ± 0.05 mag are presented as dashed lines. The objects used in the distance determination are identified with circles. (*b*) Similar to (*a*), but for our best-fit distance of $m - M = 11.67$ for $E(B-V) = 0.12$.

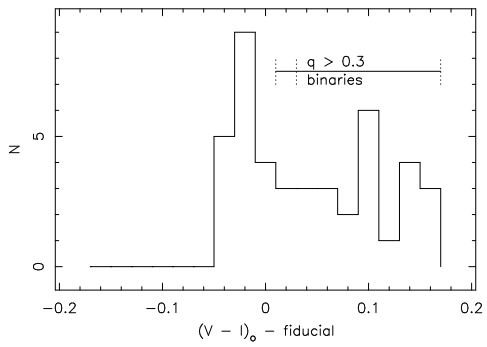

FIG. 6a

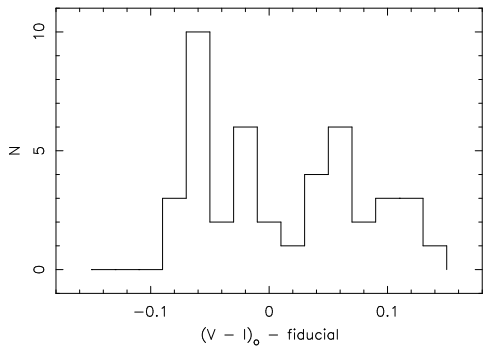

FIG. 6b

FIG. 6.—(*a*) Distribution of our selected stars about the Pinsonneault et al. (1998) fiducial main sequence for an *initial* cluster distance and reddening of $m - M = 11.41$ and $E(B-V) = 0.09$. The effect of binary star systems is clearly present in the tail of the distribution toward positive offset values. The first three or four bins contain single stars or $q \leq 0.3$ binaries, while the other bins contain $q > 0.3$ binary systems. (*b*) Similar to (*a*), but for *initial* cluster values of $m - M = 11.63$ and $E(B-V) = 0.12$.

source of external error is uncertainty in the metallicity of NGC 188. If we take the mean and range of the above-quoted three metallicity values and employ small sample statistics (Keeping 1962, p. 202), we estimate the metallicity of NGC 188 to be -0.04 ± 0.05 (standard error in the mean). Alternatively, we could rely solely on the best recent spectroscopic metallicity estimate, which is -0.12 ± 0.16 (Hobbs et al. 1990). Both means of determining the cluster metallicity provide values that are solar to within the errors and so we will not make a metallicity correction. We note, however, that there is still necessarily uncertainty in the metallicity for NGC 188. If we take twice the standard error listed above (i.e., ± 0.10) as representative of this uncertainty, this leads to a systematic uncertainty in the distance of 0.06 mag (Pinsonneault et al. 1998). Combining all of these sources of error in quadrature, we estimate that the distance modulus to NGC 188 is 11.43 ± 0.08 for $E(B-V) = 0.09$, with the largest single source of error being the uncertainty in the cluster metallicity.

3.2. *Removing Field Star Contamination*

Although the cluster main sequence is obvious in Figure 4, especially at the brighter magnitudes, a moderate number of field stars are also apparent throughout the CMD. Most of the field stars are fainter than the cluster main sequence, which is as expected since the volume surveyed increases with distance. The vast majority of the field star contamination is caused by main-sequence stars from the Galactic disk, though a few thick disk and halo main-sequence stars most likely also are present. Since some Galactic field stars overlap the position of the main sequence, a procedure is required to remove, at least statistically, the Galactic field star component. The standard procedure of statistical field star removal is to observe a comparably deep field outside the cluster at the same Galactic latitude. Because of the difficulties we had in obtaining these data, we were unable to obtain a comparison field. Nonetheless, at least for our purposes (extracting the cluster main sequence and white dwarfs), we can adequately subtract field stars with the aid of Galaxy models. Figure 7 shows the CMD for the Galaxy model of Reid & Majewski (1993) for the location, sky coverage, and reddening of our NGC 188 field. This model has been tested against north Galactic pole number counts and color distributions (Reid & Majewski 1993) and against two deep, lower latitude fields (Reid et al. 1996). For our field the number and distribution of model field stars also appear very similar to the observed distribution of field stars in Figure 4. The only location in the CMD where there appears to be some disagreement is for stars considerably redder than the NGC 188 main sequence. These objects are unlikely to be cluster members, yet no comparable population is seen in the Reid & Majewski Galaxy model. Despite these missing model stars, for our purposes the Reid & Majewski model does an excellent job of mimicking the observed cluster field stars. As an additional check we also calculated the same Galaxy field CMD with the Gilmore, Reid, & Hewitt (1985; see also Gilmore, Wyse, & Kuijken 1989) Galaxy model. Although the Gilmore et al. model provides $B-V$ colors, rather than $V-I$ colors, we carefully mapped $B-V$ to $V-I$ for main-sequence stars and found the two model CMDs to give essentially identical results for our field.

Our procedure for determining the cluster main-sequence luminosity function (LF) was to first isolate the region of the observed CMD that contained the cluster main sequence, then to isolate the same region in the Reid & Majewski model CMD. We then subtracted the model population from the observed population in 0.5 mag bins. This procedure should be insensitive to precisely how we isolate the main sequence in the CMD as long as we do not isolate too narrow a region and thereby miss some of the observed main-sequence stars. Isolating an overly large portion of the CMD will cause us to count more real field stars and more model field stars, but the difference between the two is still the number of NGC 188 main-sequence stars. We thus chose to consider main-sequence cluster members to reside

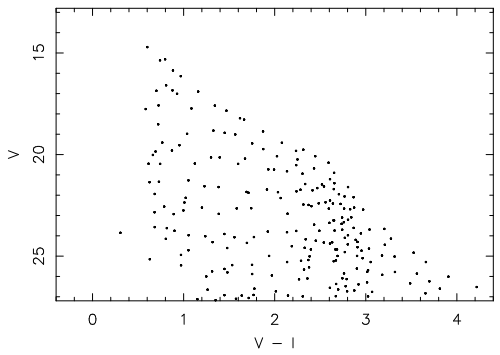

FIG. 7.—Color-magnitude diagram in V and I from the Reid & Majewski Galaxy model for the field location and size of NGC 188. This model population serves as our field star sample.

throughout a somewhat larger area than one might draw by eye, bounded on the blue side by a line starting at (V, $V-I$) = (15, 0.2) and bounded on the red side by a line with the same slope shifted by $V-I = 0.7$ redward. The turnoff region and stars brighter than $V = 15$ were included in their entirety, although two or three of these stars may be nonmembers. Before continuing on to present the cluster luminosity function, we take up the important issue of observational completeness.

3.3. *Determining Completeness*

In order to interpret the cluster luminosity function in an astrophysically useful manner, we must understand and account for the photometric completeness of the data. This means that we need to determine the efficiency of our star detection and measurement procedure at each magnitude. To accomplish this we adopted the standard approach of artificial-star experiments. The general idea is to construct a set of artificial stars with known magnitudes and positions, place these on the cluster frames, and reduce the resulting images in precisely the same manner as the original data.

We began by constructing a fiducial of the NGC 188 main sequence extending from $V = 15$ to $V = 26$. We selected stars on the fiducial sequence in half-magnitude bins between $15 < V < 20$ and quarter-magnitude bins between $20 < V < 26$. Each bin in the former magnitude range contains 38 artificial stars and each bin in the latter contains 24 such stars, totaling to 956 artificial stars. The positions of these stars were randomly generated but were constrained not to fall within 1.5 PSF radii of each other. These stars were then placed on each of the frames using the ADDSTAR routine in DAOPHOT II (Stetson 1994), which incorporates the appropriate amount of noise. The resulting frames were reduced using exactly the same procedure as the original ones. After comparing the input into the artificial-star tests with the output, we derive the relative completeness curves shown in Figures 8*a* and 8*b*. We find that the LFs are $\geq 50\%$ complete at $V = 24.6$ ($I = 21.5$).

3.4. *The Main-Sequence Luminosity Function*

We chose to study and compare the NGC 188 LF with the LFs of other stellar populations, rather than convert these LFs to mass functions, because of the well-known sensitivity of mass functions to the exact shape of the uncertain mass-luminosity relation. The data presented in Figure 4 show the main sequence of NGC 188 extending to $V \approx 25$, where it becomes difficult to distinguish from the contaminating Galactic field stars. It is clear, however, that the luminosity function drops markedly for magnitudes fainter than $V \approx 18$ and that an extensive binary sequence exists to the limit of the data. The cluster and model field star LFs, as discussed above, are presented in Figures 8*a* and 8*b* (V and I, respectively). The model Galaxy contribution increases slowly with magnitude, but until the observations begin to suffer from incompleteness the model field contribution is always small compared with the observed

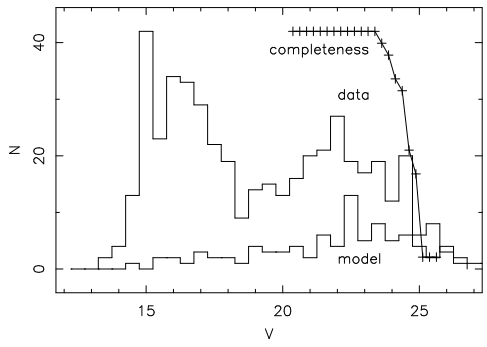

FIG. 8*a*

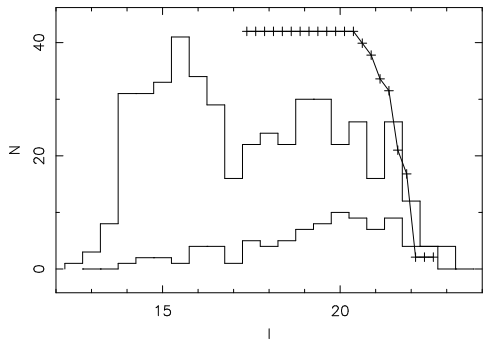

FIG. 8*b*

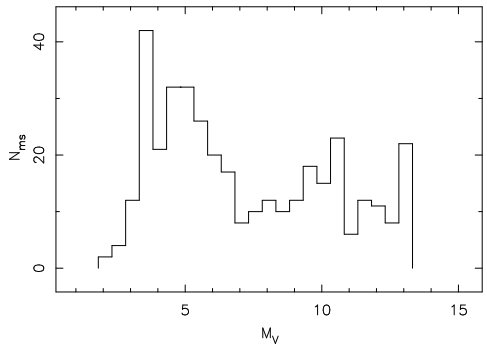

FIG. 8*c*

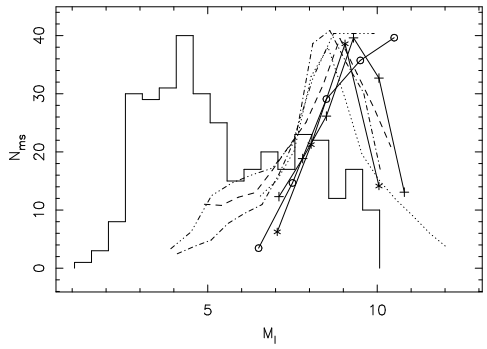

FIG. 8*d*

FIG. 8.—(*a*) The upper histogram marked "data" is the V-band luminosity function of observed cluster and field stars selected to have colors and magnitudes near the fiducial main sequence of NGC 188. The lower histogram marked "model" is the V-band luminosity function of model field stars with the same colors and magnitudes from the Reid & Majewski Galaxy model. The completeness fraction is shown as the solid line overplotting the plus signs, dropping from 1.0 near $V = 20$ to 0.0 near $V = 25$. (*b*) Similar to (*a*), but for the I band. (*c*) Absolute magnitude V-band main-sequence luminosity function derived from the completeness-corrected difference between the observed CMD counts and the Reid & Majewski model CMD counts and based on the cluster distance and reddening. (*d*) Similar to (*c*), but for the I band. In addition, a number of other LFs are overplotted: the solid line with the plus signs for the solar neighborhood, the solid lines with circles for NGC 2477, the solid lines with asterisks for NGC 2420, the dotted line for NGC 6397, the dashed line for 47 Tuc, the dash–single-dotted line for M15, and the dash–double-dotted line for ω Cen. Some of the globular cluster LFs are on the M_{814} (*HST* I-band magnitude) system, but this is very close to the standard Cousins I-band magnitude system. The cluster LFs have been scaled to fit on the same plot.

number counts. The field star correction is thus modest, and reasonable errors in the Reid & Majewski model should not affect the overall results. Figures 8*c* and 8*d* present the completeness-corrected differences between the LFs of Figures 8*a* and 8*b*, respectively, with the *x*-axes now in absolute rather than apparent magnitudes. The *V*- and *I*-band LFs both peak at M_V and M_I in the range of 3–4 and are plotted only where completeness is $\geq 50\%$. These LFs are unlike the solar neighborhood LF and unlike the LFs from a broad range of open and globular clusters chosen such that mass segregation and other dynamical processes are unimportant. A number of such representative LFs (ω Cen from Elson et al. 1995; 47 Tuc from De Marchi & Paresce 1995b; M15 from De Marchi & Paresce 1995a; NGC 6397 from Paresce, De Marchi, & Romaniello 1995; NGC 2420 and NGC 2477 from von Hippel et al. 1996; the solar neighborhood from Kroupa, Tout, & Gilmore 1993) are plotted in Figure 8*d*, where it can be seen that they typically rise continuously until $M_I \approx 9.5$.

The above analysis presents the NGC 188 LF under the assumption that all main-sequence objects are single stars. We can tell from a casual glance at Figure 4, however, that for NGC 188 this is incorrect; the cluster has a large population of binary star systems. Open clusters typically have a large fraction of binaries, while globular clusters typically have far fewer ($\lesssim 10\%$; e.g., Richer et al. 1997 and references therein). The general effect of counting multiple star systems as single stars in an LF is to overestimate the brightness of many stars and to underestimate the contribution of low-mass members. While this is undoubtedly causing the observed NGC 188 LF to be unrepresentative of its underlying population, this problem also occurs to a similar degree in the observed LFs for NGC 2420 and NGC 2477. These open cluster LFs look nothing like the NGC 188 LF, so although binaries may play a role in changing the LF shape they are not responsible for the great differences seen between LF shapes in Figure 8*d*.

While the statistical subtraction technique employed above does not allow us to identify individual single and binary cluster members, it does allow us to estimate the fractional contribution of binary stars. The distribution of objects within 0.2 mag of the fiducial main sequence has already been plotted in Figure 6 within the limited color range of $0.8 \leq V-I \leq 1.0$, corresponding to the range $16.3 \leq V \leq 17.3$. This region appears to the eye to have approximately the same binary contribution as fainter portions of the main sequence, and the greater number of stars in this region make any fractional determination more robust than at fainter magnitudes. Examining Figure 6*a* we find 18 (21) stars in the leftmost three (four) bins, while the remainder of the bins have 25 (22) stars. These numbers are equal within their uncertainty. Since the number gradient of field stars across the main sequence is small, we assume the background field contributes equally to the identified single and binary distributions. We find that $\sim 50\%$ of main-sequence stars within 0.2 mag of the main sequence are single stars or have low enough mass ratios ($q \leq 0.3$; see Pols & Marinus 1994) to appear single and that the remaining $\sim 50\%$ are multiple systems. More multiple star systems are likely present at greater luminosity separation from the main sequence, up to at least 0.75 mag, the expected offset caused by two equal-mass binary members. We assume the binary fraction we measure is thus a lower limit for the $0.8 \leq V-I \leq 1.0$ color region and we further assume that this region of the main sequence is typical of the cluster. We conclude that at least 50% of the cluster objects are binaries.

Since the LFs presented here come from a single central cluster field it is difficult to determine whether the deficit of low-mass stars is due simply to mass segregation (i.e., the low-mass cluster members still belong to the cluster but occupy a much larger volume), whether a significant number of low-mass members have been dynamically ejected, or whether the cluster always had a deficit of low-mass members. This last possibility, that NGC 188 was created with a deficit of low-mass members, is unlikely, however, since clusters with overly flat initial mass functions are dynamically unstable (Terlevich 1987; Vesperini & Heggie 1997). In addition, on observational grounds (see von Hippel et al. 1996; von Hippel 1998) little variation is seen between cluster mass functions for cases where one can isolate a sample that has suffered little dynamical evolution. The case for dynamical evolution for NGC 188 is strong. Other authors (e.g., Dinescu et al. 1996) have noted the advanced dynamical state of the cluster, which is to be expected from its great age. In fact, the vast majority of open clusters do not survive to nearly the age of this cluster. McClure & Twarog (1977) give a relaxation time for NGC 188 of 6.4×10^7 yr and Binney & Tremaine (1987, p. 491) note that cluster evaporation times are typically 100 times their relaxation time, i.e., essentially the age of the cluster.

Finally, we note that the expected number of background contaminating galaxies (see below) in the faint main-sequence portion of our cluster is essentially zero, since very few galaxies are as red as $V-I \approx 3$.

3.5. *White Dwarfs*

We now turn to a study of the white dwarf region of the CMD (Figs. 4 and 9), where we identify nine candidate WDs. These nine candidate WDs are identified by overplotted circles in Figure 9, which is the dereddened CMD with the distance modulus of 11.43 subtracted. [There are two WD candidates at $(V-I,\ M_V) = (-0.04,\ 12.06)$ and $(-0.03,\ 12.08)$, so only eight distinct objects are visible in the CMD]. Also plotted in this figure is the observed solar neighborhood WD sequence of Monet et al. (1992) and the

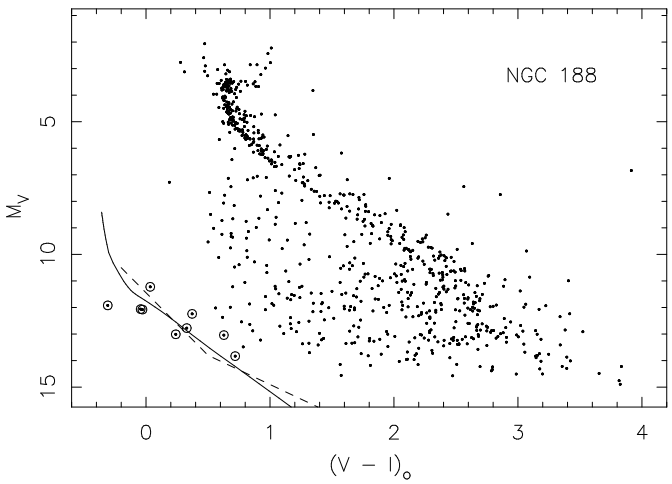

FIG. 9.—Dereddened color-magnitude diagram of Fig. 4 with distance removed. The nine candidate WDs (two overlap) are identified by overplotted circles. In addition to the observed Monet et al. (1992) WD sequence, the log $g = 8$ hydrogen atmosphere theoretical WD cooling sequence of Bergeron et al. (1995) is plotted (*solid line*).

log $g = 8$, hydrogen atmosphere theoretical WD cooling sequence of Bergeron, Wesemael, & Beauchamp (1995). The candidate WDs were identified based on their photometric proximity to the Monet et al. and Bergeron et al. cooling sequences. We also visually inspected the location of the WD candidates on the images. Some of the candidates were too faint to visually ensure that they were not instrumental artifacts. We believe ALLFRAME can more reliably compare signals from multiple V- and I-band images than we can do visually, and so we believe all or most of our nine WD candidates are real objects. However, three of the WD candidates (WD5, WD8, and WD9; see Table 2) have a somewhat lower likelihood of being cluster WDs either because of their distance from the WD loci (candidate WD5 is 2 σ distant in $V-I$) or because they have similar V and I magnitudes to the more abundant field stars (candidates WD8 and WD9). The Reid & Majewski and Gilmore et al. Galaxy models also allow us to estimate the expected field star contamination in the WD region. The Reid & Majewski model predicts that two or perhaps three Galactic field WDs would lie in the same region of the CMD as the cluster WDs. The Gilmore et al. model similarly predicts that one or two Galactic field WDs would lie in the same region of the CMD as cluster WD candidates. Despite this possible contamination, the nine candidate WDs significantly exceed the expected number (two or three) of non-cluster stars with similar colors. A reasonable upper limit to the number of candidate WDs that are true cluster WDs is six, with the three most tentative candidate objects mentioned above being identified as the expected interlopers predicted by the Reid & Majewski and Gilmore et al. Galaxy models. A reasonable lower limit is probably three WDs. In this case the poorer candidates are field main-sequence stars and another three objects nearer the WD sequence are field WDs as predicted by the Galaxy models.

In the above discussion we have ignored the possible contribution of unresolved background galaxies. Although the number of background galaxies in any deep field is large, we have two methods to discriminate against them. Our first method is to rely on image morphology since many, and perhaps most, galaxies are at least marginally resolved in our best seeing (0.″7) images. In a study of deep galaxy counts, Smail et al. (1995; see their Fig. 4) demonstrate that the stellar locus is almost completely distinguishable from galaxies down to $R = 24$ ($V = 24.5$ for the average background galaxy). While their images were obtained during both better seeing (0.″5 to 0.″6 vs. 0.″7) and higher signal-to-noise ratio than ours, it seems safe to assume that our conservative morphological discrimination should remove 90%–95% of the background galaxies. Our second method is to rely on color selection. Fortunately for the white dwarf study, there are few faint galaxies with colors near the best WD candidates, $V-I = 0.0$ to 0.4. Smail et al. (1995) find that 95% of galaxies at $V \approx 24.5$ lie within a color range a few tenths of a magnitude bluer than $V-I \approx 1.0$. They do not report the fraction as blue as our WD candidates, but it seems safe to assume that number to be much less than 1%. Our two discriminatory tools should thus reduce the contaminating background galaxy count by a factor of at least 10^3. The number of background galaxies per magnitude reported by Smail et al. at $V = 24.5$, when scaled to the size of the WIYN S2KB field of view (0.0129 deg^2), corresponds to $\sim$650 objects. The expected contamination in the WD region is therefore less than one object. Of course, tracing the WD sequence to fainter flux levels and redder colors would make this problem increasingly difficult, since the number of background galaxies increases dramatically at fainter magnitudes, and since the color discrimination would markedly diminish.

Observed and derived properties for the nine WD candidates are listed in Table 2. The derived properties are based on the models of Bergeron et al. (1995) under the assumption that each object is indeed a white dwarf. For each WD candidate, Table 2 lists the candidate name in the IAU R.A. + decl. style in column (1), a shorter alias we will use in this paper in column (2), the dereddened $V-I$ color in column (3), the absolute V-band magnitude in column (4), the effective temperature in kelvins in column (5), the WD mass in solar masses in column (6), the absolute bolometric magnitude in column (7), and the logarithm of the age in years in column (8). Columns (4), (5), (7), and (8) also list errors in the observed and derived quantities in parentheses. The errors in the derived quantities are based on propagating the observed photometric errors through the Bergeron et al. model calibrations; as such, they are internal errors only. No errors are listed for the derived quantity of mass

TABLE 2

PARAMETERS FOR CANDIDATE WHITE DWARFS

Name (1)	Alias (2)	$(V-I)_0$ (3)	M_V (4)	$T_{\rm eff}$ (5)	Mass (6)	$M_{\rm bol}$ (7)	log (Age) (8)	Model (9)
WOCS J0048511+851153.....	WD1	0.03	11.22 (0.035)	15115 (301)	0.614	10.00 (0.088)	8.339 (0.025)	H
				15336 (234)	0.588	9.99 (0.065)	8.376 (0.023)	He
WOCS J0049422+851208.....	WD2	−0.31	11.92 (0.043)	10720 (152)	0.604	11.51 (0.062)	8.735 (0.016)	H
				11443 (196)	0.580	11.28 (0.075)	8.768 (0.021)	He
WOCS J0050018+851709.....	WD3	−0.04	12.06 (0.044)	10265 (132)	0.604	11.71 (0.056)	8.782 (0.014)	H
				10835 (169)	0.579	11.52 (0.070)	8.834 (0.019)	He
WOCS J0050137+851214.....	WD4	−0.03	12.08 (0.044)	10212 (132)	0.603	11.73 (0.057)	8.788 (0.014)	H
				10768 (168)	0.579	11.54 (0.070)	8.841 (0.019)	He
WOCS J0050123+851704.....	WD5	0.37	12.24 (0.046)	9763 (120)	0.602	11.93 (0.054)	8.837 (0.013)	H
				10149 (174)	0.579	11.80 (0.073)	8.910 (0.019)	He
WOCS J0049562+851236.....	WD6	0.33	12.78 (0.061)	8495 (132)	0.598	12.54 (0.069)	8.989 (0.017)	H
				8486 (158)	0.575	12.58 (0.081)	9.108 (0.020)	He
WOCS J0050050+851827.....	WD7	0.24	13.01 (0.076)	8003 (156)	0.597	12.80 (0.085)	9.055 (0.022)	H
				7923 (172)	0.575	12.88 (0.095)	9.184 (0.024)	He
WOCS J0048348+851836.....	WD8	0.63	13.04 (0.078)	7943 (158)	0.597	12.83 (0.088)	9.064 (0.022)	H
				7857 (172)	0.575	12.92 (0.095)	9.193 (0.024)	He
WOCS J0046171+851756.....	WD9	0.72	13.83 (0.147)	6516 (225)	0.592	13.70 (0.152)	9.280 (0.037)	H
				6407 (220)	0.574	13.81 (0.150)	9.411 (0.035)	He

since formally the error is always 0.001 $M_\odot$. Note that the mass values are the result of using models with fixed log $g = 8$, and not the result of determining the expected mass for each WD based on the cluster age and WD cooling ages. Nonetheless, the derived WD masses are all nearly 0.6 $M_\odot$, and these minor variations are unimportant for our purpose, which is to comment generally on the white dwarf ages. The derived quantities are listed twice, based first on hydrogen and then on helium atmosphere models, as indicated in column (9). The vast majority of spectroscopically observed WDs have hydrogen atmospheres, so these are the numbers we expect to be relevant for NGC 188. The helium atmosphere results are included to demonstrate the size of the effect of this basic change in the WD parameters.

If all the objects listed in Table 2 are cluster WDs, then NGC 188 must be at least as old as its faintest WD. The lower age limit would be 1.91 ± 0.16 Gyr (H atmosphere result) or 2.58 ± 0.21 Gyr (He atmosphere result). Objects WD6 and WD7 are much more reliable than object WD9 or even WD8, however. For the most likely situation of hydrogen atmospheres, these objects are aged 0.98 ± 0.04 and 1.14 ± 0.06 Gyr. The cluster distance uncertainty of ± 0.08 increases these age uncertainties slightly, to ± 0.06 and ± 0.09 Gyr, respectively. The WD cooling ages are not surprising, since the accepted age for NGC 188 is ≈ 6 Gyr. Observations probing to $V = 27$ or 28 will be necessary to find the faintest cluster WDs. These faintest cluster WDs will be both redder and superposed on yet more background objects, however, limiting the efficacy of the simple photometric technique employed here. A third filter sensitive to the calcium H and K lines in the background stars may help, though deep observations with such a narrow-band filter will be time-consuming. Proper motions may also help, though the proper-motion difference between NGC 188 and the Galactic field is only ~ 1 mas yr^{-1} (Méndez & van Altena 1996), requiring a 10 or 20 yr delay before a meaningful second epoch could be obtained. Perhaps the best means of obtaining the WD sequence terminus would be to observe essentially the entire cluster. NGC 188 is expected to have $\geq 6\%$ by mass of its stars in the form of WDs (von Hippel 1998). For a cluster dynamically evolved from an IMF with a Salpeter-like slope, the number fraction of WDs should be at least as great as the mass fraction. The proper-motion study of Dinescu et al. (1996) found 360 cluster members to $B = 16.2$, so it seems reasonable to assume that at least 1000 cluster members exist (see, for comparison, the V-band LF in Fig. 8*a*). Since more than 50% of cooling WDs pile up near the terminus of the WD sequence, we expect ≥ 30 WDs to define this cooling sequence terminus, and they should thus be observable as an excess even against a significant background contamination.

Although we have not been able to find the faintest WDs in NGC 188, our result demonstrates the value of the WD age technique and its very low internal errors. While observationally difficult, the theoretical age determination based on WD luminosities, once a good cluster WD sample has been isolated, is much less troublesome than the theoretical age determination based on isochrone fitting to the main-sequence turnoff.

4. CONCLUSION

We have employed precise and carefully calibrated V- and I-band photometry of NGC 188 at WIYN Observatory to explore the cluster luminosity function and study the cluster white dwarfs. Our observations span more than 1 yr and include a single night tied to the Landolt (1992) Johnson-Kron-Cousins photometric system to within 0.01 mag. Photometric bootstrapping procedures were employed to calibrate the faint stars from the remainder of the nights to the single calibrated night, and the total external systematic in the faint star calibration should be ≤ 0.032 mag. Our photometry is offset by $V = 0.052$ (fainter) from Sandage (1962) and Eggen & Sandage (1969). Since all photometry for the past three decades has been tied to Sandage (1962) and Eggen & Sandage (1969), all past photometry includes a 0.05 ± 0.01 mag photometric zero-point error.

We employ the Pinsonneault et al. (1998) fiducial open cluster main sequence to derive distance moduli to NGC 188 based on the two most frequently used cluster reddening values, $E(B-V) = 0.09$ and 0.12. Our best-fit distance moduli are $m - M = 11.43$ for $E(B-V) = 0.09$ and $m - M = 11.67$ for $E(B-V) = 0.12$. Based on past distance estimates to NGC 188 (see Twarog et al. 1997), we favor the $E(B-V) = 0.09$ result. Carefully considering a variety of sources of external error, we estimate that the NGC 188 distance modulus is 11.43 ± 0.08 and $E(B-V) = 0.09$, with the largest single source of uncertainty being the uncertainty in the metallicity of the cluster.

In order to determine the cluster luminosity function, we employ the Galaxy model of Reid & Majewski (1993) to determine the number of contaminating field stars. We find this technique works well. We also find that our morphological (0.″7 seeing) and color selections decrease the expected extragalactic contamination to less than one object in either the white dwarf or main-sequence regions of the CMD. We employ the standard approach of artificial-star experiments to estimate completeness and find our observations are $\geq 50\%$ complete along the main sequence to $V = 24.6$. After determining the small field star and completeness corrections, we find that the NGC 188 central-field LF peaks at $M_I \approx 3$ to 4. This is unlike the solar neighborhood LF and unlike the LFs of dynamically unevolved portions of open and globular clusters, all of which typically rise continuously until $M_I \approx 9.5$. Although we find that $\geq 50\%$ of the unresolved objects in this central cluster field are multiple systems with mass ratios ≥ 0.3, their presence cannot account for the shape of the NGC 188 LF. For theoretical reasons (Terlevich 1987; Vesperini & Heggie 1997) having to do with the long-term survivability of NGC 188 (McClure & Twarog 1977; Binney & Tremaine 1987), we believe the cluster had a typical IMF, but that it is now highly dynamically evolved and the missing low-luminosity stars are either in the cluster outskirts or have left the cluster altogether.

We identify nine candidate WDs in NGC 188, of which we expect at least three, and perhaps six, are bona fide cluster WDs. The luminosities of the faintest likely WD indicate an age (Bergeron et al. 1995) of 1.14 ± 0.09 Gyr, where the error in age includes the cluster distance uncertainty and we assume the WD has a hydrogen atmosphere. This age is a lower limit to the cluster age, and observations probing to $V = 27$ or 28 will be necessary to find the faintest cluster WDs and independently determine the cluster age. While our lower age limit is not surprising, since the accepted cluster age is ≈ 6 Gyr, our result demonstrates the value of the WD age technique with its very low internal errors. While observationally difficult, the theoretical age

determination based on WD luminosities, once a good cluster WD sample has been isolated, is much less troublesome than the theoretical age determination based on isochrone fitting to the main-sequence turnoff.

We thank Betsy Green for many useful discussions and help with calibration issues. We thank Imants Platais for helpful discussions, providing the astrometry, and naming conventions. We also thank Con Deliyannis, Pierre Demarque, Bob Mathieu, and an anonymous referee for helpful comments on the manuscript. T. v. H. expresses his appreciation for grant support provided by the Edgar P. and Nona B. McKinney Charitable Trust. A. S. expresses his gratitude to UCO/Lick Observatory for kind hospitality during his visit. A. S. was supported by the National Aeronautics and Space Administration (NASA) grant HF-01077.01-94A from the Space Telescope Science Institute, which is operated by the Association of Universities for Research in Astronomy, Inc., under NASA contract NAS 5-26555.

REFERENCES

Baliunas, S. L., & Guinan, E. F. 1985, ApJ, 294, 207
Bergeron, P., Wesemael, F., & Beauchamp, A. 1995, PASP, 107, 1047
Bertin, E., & Arnouts, S. 1996, A&AS, 117, 393
Binney, J., & Tremaine, S. 1987, Galactic Dynamics (Princeton: Princeton Univ. Press)
Caputo, F., Chieffi, A., Castellani, V., Collados, M., Martinez Roger, C., & Paez, E. 1990, AJ, 99, 261
Cardelli, J. A., Clayton, G. C., & Mathis, J. S. 1989, ApJ, 345, 245
Carraro, G., & Chiosi, C. 1994, A&A, 288, 751
Carraro, G., Chiosi, C., Bressan, A., & Bertelli, G. 1994, A&A, 103, 375
De Marchi, G., & Paresce, F. 1995a, A&A, 304, 202
———. 1995b, A&A, 304, 211
Demarque, P., Green, E. M., & Guenther, D. B. 1992, AJ, 103, 151
Dinescu, D. I., Demarque, P., Guenther, D. B., & Pinsonneault, M. H. 1995, AJ, 109, 2090
Dinescu, D. I., Girard, T. M., van Altena, W. F., Yang, T.-G., & Lee, Y.-W. 1996, AJ, 111, 1205
Eggen, O. J., & Sandage, A. R. 1969, ApJ, 158, 669
Elson, R. A. W., Gilmore, G. F., Santiago, B. X., & Casertano, S. 1995, ApJ, 110, 682
ESA. 1997, The Hipparcos and Tycho Catalogues (ESA SP-1200) (Noordwijk: ESA)
Gilmore, G., Reid, I. M., & Hewitt, P. C. 1985, MNRAS, 213, 257
Gilmore, G., Wyse, R. F. G., & Kuijken, K. 1989, ARA&A, 27, 555
Harris, W. E., Fitzgerald, M. P., & Reed, B. C. 1981, PASP, 93, 507
Henry, T. J., & McCarthy, D. W. 1993, AJ, 106, 773
Hobbs, L. M., & Pilachowski, C. 1988, ApJ, 334, 734
Hobbs, L. M., Thorburn, J. A., & Rodriguez-Bell, T. 1990, AJ, 100, 710
Kaluzny, J. 1990, Acta Astron., 40, 61
Kaluzny, J., & Shara, M. M. 1987, ApJ, 314, 585
Keenan, D. W., Innanen, K. A., & House, F. C. 1973, AJ, 78, 173
Keeping, E. S. 1962, Introduction to Statistical Inference (Princeton: Van Nostrand)
Kroupa, P., Tout, C. A., & Gilmore, G. 1993, MNRAS, 262, 545
Landolt, A. U. 1983, AJ, 88, 439
———. 1992, AJ, 104, 340
Leonard, P. J. T., & Linnell, A. P. 1992, AJ, 103, 1928
Massey, P., Jacoby, G., Carder, E., & Harris, H. 1987, NOAO Newsl., 12, 28
Mathieu, R. D., & Dolan, C. 1998, in preparation
McClure, R. D., & Twarog, B. A. 1977, ApJ, 214, 111
Méndez, R. A., & van Altena, W. F. 1996, AJ, 112, 655
Monet, D. G., Dahn, C. C., Vrba, F. J., Harris, H. C., Pier, J. R., Luginbuhl, C. B., & Ables, H. D. 1992, AJ, 103, 638
Moss, D. 1985, A&A, 150, 343
Norris, J., & Smith, G. H. 1985, AJ, 90, 2526
Paresce, F., De Marchi, G., & Romaniello, M. 1995, ApJ, 440, 216
Phelps, R., Janes, K. A., & Montgomery, K. A. 1994, AJ, 107, 1079
Pinsonneault, M. H., Stauffer, J., Soderblom, D. R., King, J. R., & Hanson, R. B. 1998, ApJ, 504, 170
Pols, O. R., & Marinus, M. 1994, A&A, 288, 475
Reid, I. N., & Majewski, S. R. 1993, ApJ, 409, 635
Reid, I. N., Yan, L., Majewski, S., Thompson, I., & Smail, I. 1996, AJ, 112, 1472
Richer, H. B., et al. 1997, ApJ, 484, 741
Sandage, A. 1962, ApJ, 135, 333
Scott, J. E., Friel, E. D., & Janes, K. A. 1995, AJ, 109, 1706
Smail, I., Hogg, D. W., Yan, L., & Cohen, J. G. 1995, ApJ, 449, L105
Spinrad, H., Greenstein, J. L., Taylor, B. J., & King, I. R. 1970, ApJ, 162, 891
Spinrad, H., & Taylor, B. J. 1969, ApJ, 157, 1279
Stetson, P. B. 1994, PASP, 106, 250
Terlevich, E. 1987, MNRAS, 224, 193
Tody, D. 1993, in ASP Conf. Ser. 52, Astronomical Data Analysis Software and Systems II, ed. R. J. Hanisch, R. J. V. Brissenden, & J. Barnes (San Francisco: ASP), 173
Twarog, B. A. 1978, ApJ, 220, 890
Twarog, B. A., & Anthony-Twarog, B. J. 1989, AJ, 97, 759
Twarog, B. A., Ashman, K. M., & Anthony-Twarog, B. J. 1997, AJ, 114, 2556
Upgren, A. R., Mesrobian, W. S., & Kerridge, S. J. 1972, AJ, 77, 74
van 't Veer, F. 1984, A&A, 139, 477
Vesperini, E., & Heggie, D. C. 1997, MNRAS, 289, 898
von Hippel, T. 1998, AJ, 115, 1536
von Hippel, T., Gilmore, G., & Jones, D. H. P. 1995, MNRAS, 273, L39
von Hippel, T., Gilmore, G., Tanvir, N., Robinson, D., & Jones, D. H. P. 1996, AJ, 112, 192